Available online at www.sciencedirect.com
ScienceDirect
Trans. Nonferrous Met. Soc. China 31(2021) 865−877
Transactions of Nonferrous Metals Society of China
www.tnmsc.cn

Eliminating shrinkage defects and improving mechanical performance of large thin-walled ZL205A alloy castings by coupling travelling magnetic fields with sequential solidification

Lei LUO, Hong-ying XIA, Liang-shun LUO, Yan-qing SU, Chao-jun CAI, Liang WANG, Jing-jie GUO, Heng-zhi FU

National Key Laboratory for Precision Hot Processing of Metals, School of Materials Science and Engineering, Harbin Institute of Technology, Harbin 150001, China

Received 16 May 2020; accepted 22 December 2020

Abstract: ZL205A alloys with large thin-walled shape were continuously processed by coupling travelling magnetic fields (TMF) with sequential solidification, to eliminate the shrinkage defects and optimize the mechanical performance. Through experiments and simulations, the parameter optimization of TMF and the influence on feeding behavior, microstructure and properties were systematically studied. The results indicate that the magnetic force maximizes at the excitation current of 20 A and frequency of 200 Hz under the experimental conditions of this study, and increases from center to side-walls, which is more convenient to process thin-walled castings. TMF can break secondary dendritic arm and dendrites overlaps, widen feeding channels, prolong the feeding time, optimize the feeding paths, eliminate shrinkage defects and improve properties. Specifically, for as-cast state, TMF with excitation current of 20 A increases ultimate tensile strength, elongation and micro-hardness from 186 MPa, 7.3% and 82.1 kg/mm^2 to 221 MPa, 11.7% and 100.5 kg/mm^2, decreases porosity from 1.71% to 0.22%, and alters brittle fracture to ductile fracture.

Key words: ZL205A alloys; large thin-walled alloy castings; travelling magnetic fields; sequential solidification; shrinkage defects; mechanical performance

1 Introduction

ZL205A alloys are the Al−Cu based alloys with the outstanding comprehensive mechanical properties such as the low density, high specific strength, ductility and toughness [1,2]. Accordingly, they are extensively employed in the automobiles, aerospace, aviation and military fields, and especially used as large thin-walled castings [3,4]. While, continuous casting is one of the main forming methods for large castings being explored [5]. However, during the continuous casting process, the large solidification intervals of ZL205A alloys, i.e., the difference between the liquid and solid temperatures, are prone to inducing the unstable solid−liquid interface to form cellular and dendritic crystals [6−9] and easily forming the compositional undercooling in mushy zones, so that the deflected and disordered growth of the primary dendrites ensues, accompanied by the prolific formation of the secondary dendrites [10]. In this case, the feeding channels between the dendrites in the mushy zones become blocked, resulting in the increase of the shrinkage defects [11−13]. Additionally, all these results are more harmful to the large thin-walled alloy castings, because the melt flows and feeding capacity are seriously restricted and reduced due to their size and shape. Ultimately, the mechanical properties, production efficiency and material utilization will be slashed. Consequently, finding ways to

Corresponding author: Yan-qing SU; Tel: +86-451-86418740; E-mail: suyq@hit.edu.cn
DOI: 10.1016/S1003-6326(21)65545-0

effectively solve the feeding problems and improve the mechanical performance of the large thin-walled ZL205A alloy castings during the solidification process is of great significance.

Currently, many methods have been proposed to enhance the feeding capacity of the alloy melt, such as changing the gating system [14], altering the casting modes [15,16], regulating the melt condition [17,18] and applying external physical fields [19−21]. However, changing the gating system, altering the casting modes and regulating the melt condition will increase the complexity of the solidification process and even cause secondary pollution to the alloy melt. In addition, these methods will increase the waste of materials and the manufacturing costs. Contrastively, applying an external physical field, especially the travelling magnetic fields (TMF), is more suitable for rapid, efficient and automatic casting, because of their non-contacting, pollution-free and easily-controlled advantages [22,23]. Meanwhile, the sequential solidification (SS) process is often used as one of the most important methods to regulate the stability of the mass and heat distribution in mushy zones, and it can effectively replace the continuous casting process to obtain more stable solidification control conditions [24].

Correlational studies [25,26] have suggested that TMF processing can promote the crushing and breaking of the secondary dendrite arms, and transfer the shredded fragments to the high-temperature melt zone or the undercooled liquid region for re-melting or regenerating nucleation. Noteworthily, appropriate parameters of TMF can promote the directional growth of matrix phase α(Al) and restrict the growth of secondary dendrite together in Al−Cu based alloys [27]. Moreover, buoyancy and Marangoni forces as well as the Lorentz forces induced by TMF will generate various sequential forced melt flows instead of natural convection in the alloy melt, resulting in effective heat and mass transmission [28,29], as well as the microstructural evolution [30]. Besides, other literatures [31,32] have also proposed that magnetic fields stirring can effectively penetrate the mushy zone so as to improve the solidification feeding and eliminate the porosity. However, most of the studies focused on the rod-like samples of Al−Cu binary model alloy, regardless of the size and shape of alloys, nor of the multi-element and multi-phase of alloys. In summary, none of the current research involves applying the TMF to the ZL205A alloys castings with large solidification intervals and multi-phase, especially, with the large thin-walled shape. Therefore, the study on whether TMF can effectively improve the feeding capacity, reduce the shrinkage porosity and increase the mechanical properties of large thin-walled ZL205A alloys castings is scarce. Similarly, the influence mechanism of TMF on the feeding behavior is also relatively lacking.

In this regard, in the current work, we couple TMF with SS process to improve the feeding capability of ZL205A alloys with large solidification intervals, multi-phase and large thin-walled shapes by continuously regulating the mushy zone and solidification behavior. Furthermore, by combining the simulations with experiments, we conduct systematic studies on the optimization of the TMF parameters, and on the variations of solidification process, microstructures, and mechanical properties induced by TMF, as well as the related mechanisms. Our objective is to propose an innovative method and idea for decreasing the shrinkage defects and increasing the mechanical properties of large thin-walled castings made of ZL205A alloys with a large solidification interval, and to elaborate the mechanisms of them.

2 Experimental

2.1 Materials preparation

The ZL205A alloy samples (Al−5.0wt.%Cu−0.3wt.%Mn−0.15wt.%Ti) were prepared by a self-designed TMF processing equipment with SS function as shown in Fig. 1(a). The TMF was regulated and characterized by the alternating excitation current, of which the intensity was controlled by the Autotransformer (XTSGC1, China), while the frequency was controlled by the Variable-frequency Drive (MTB030G, China). In addition, the temperature gradient (G_T) and cooling rate (v_c) measured by several times were 2 K/mm and 0.3 K/s during the SS process. It is worth mentioning that, the temperature measurements were performed by using the combination of K-thermocouple with multichannel temperature recorder (MIK−4000D, China). Wherein, the temperature gradients (G_T) were measured by using three sets of thermocouples distributed equidistantly

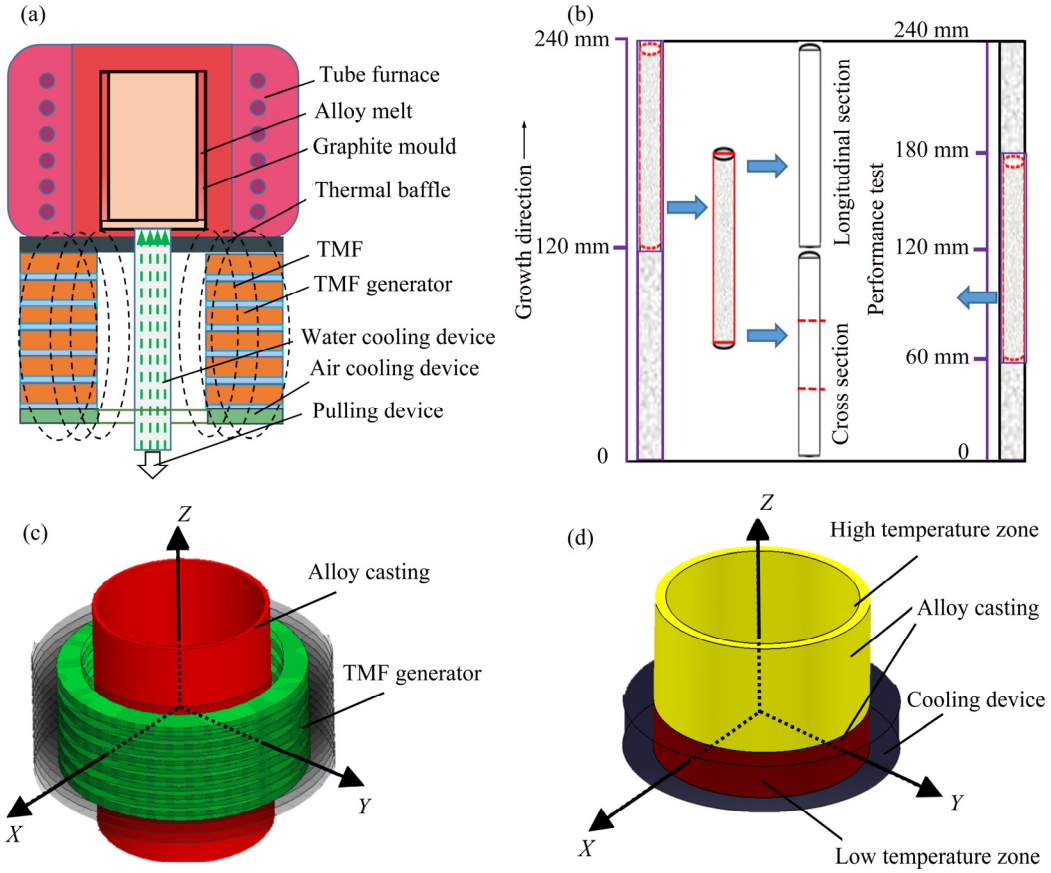

Fig. 1 Preparation schematic diagram and simulation model: (a) TMF processing equipment with SS function; (b) Selection of samples; (c) Simulation model of TMF; (d) Simulation model of SS

along the direction of temperature gradient. While, the cooling rates (v_c) were calculated by the time−temperature curves recorded by multichannel temperature recorder. Furthermore, a constant downward drag velocity (v_d=150 μm/s) was used to make sure that the solid−liquid interface can move up at the same speed as the samples move down, so as to effectively fix the mushy zones into the area of TMF. And the constant downward drag velocity (v_d) was given by

$$v_d=v_c/G_T \quad (1)$$

Each sample was melted at 1000 K in a resistance furnace and degassed with high-purity argon. After holding for 15 min, the alloy melt was poured into a cylindrical graphite mold with an inner diameter of 170 mm, an outer diameter of 180 mm and a length of 240 mm. The cylindrical graphite mold was preheated in the tube furnace at 1000 K (Fig. 1(a)), where the SS process with or without TMF was carried out. Finally, the large thin-walled castings with a wall thickness of 5 mm and a height of 240 mm were obtained by SS process with the constant downward drag velocity v_d=150 μm/s, under the different TMF processes. It is worth noting that the excitation current was used to represent the strength of the magnetic fields, because of the strong spatial and temporal dependence of TMF [33]. And the different excitation currents (I_e=0, 5, 10, 15, 20 A) were selected to perform a semi-quantitative study of the effects of TMF on the microstructure and the feeding capacity of alloys. In this study, due to the limitation of equipment, the maximum current was set to 20 A, and related laws of TMF were studied under these conditions.

2.2 Measurement and analysis methods

We selected the same positions of samples along the direction of temperature gradient to analyze the microstructure in longitudinal and cross sections, as well as the performance (Fig. 1(b)). The microstructural morphology and chemical composition were respectively analyzed by scanning electron microscopy (SEM, Quanta

200FEG, FEI, USA) and X-ray photoelectron spectroscopy (XPS, ESCALAB 250Xi, Thermo Fisher, USA). The measurements of tensile strength were performed at room temperature with a strain rate of 10^{-3} s^{-1} by universal testing machine (Instron5569, Instron, USA), and the tensile axis was chosen parallel to the direction of temperature gradient. The tensile tests were repeated 3 times and the average value was taken, of which the standard deviation was approximately 5%. Microhardness was measured by a hardness tester (HVS−1000A, Laizhou Huayin, China) with a 300 g load and dwell time of 10 s. Similarly, the average value of 10 times measurements was taken, of which the standard deviation was about 5%. The density tests of the samples were conducted by the high precision digital display density meter (QL−202GR, Shenzhen Qunlong, China); and the average of 30 times measurements was selected, of which the standard deviation was about 5%. Besides, the strength of the magnetic fields used in the experiments was measured by tesla-meter (HT201A, Shanghai Hengtong, China).

2.3 Simulations and calculations

The magnetic fields and magnetic force density were simulated by the Ansoft-Maxwell software (ANSYS Inc., USA). ESI-Procast software (ESI, FRA) was utilized to emulate the SS process, including the distributions of temperature and shrinkage defects in the alloy castings. Relevant parameters applied in the simulations are displayed in Table 1, and the simulated models are shown in Figs. 1(c) and (d). In the simulations of magnetic fields and magnetic force density, the following assumptions were made: (1) the permittivity, permeability and material conductivity involved in the calculations were assumed to be constant, regardless of the influence of temperature; (2) each set of coils was considered as a unit, with the magnetic flux leakage between each two winds neglected; (3) the refractories attached to the TMF generator and the insulation materials in the experiment were modeled as regions of vacuum, because of their low permeability and non-conductivity; (4) the heating of the melt caused by TMF was not considered in the simulations. Analogously, in the calculations of the solidification behavior produced by TMF during the SS process, the following assumptions were made: (1) MILE algorithm was used to simulate the SS process; (2) the magnetic force added into the alloy melt were regarded as the average magnetic force; (3) the average magnetic force applied to each position in the melt was considered as equal; (4) the Niyama criterion was used to represent the quantity of shrinkage defects.

Table 1 Related parameters used in simulations of magnetic fields and solidification behavior [27]

Parameter	Symbol	Value
TMF inner diameter	D_i/mm	200
TMF outer diameter	D_o/mm	400
Number of windings	n	100
Phase angle	φ	0, 2π/3, 4π/3
Temperature gradient	G_T/(K·mm^{-1})	2
Cooling rate of alloys	v_c/(K·s^{-1})	0.3
Thermal conductivity	C_T/(W·m^{-1}·K^{-1})	236
Magnetic permeability	μ_{Al}/(H·m^{-1})	1
Electrical conductance	σ_e/(S·m^{-1})	35.3×10^6
Density of alloy melt	ρ/(kg·m^{-3})	2614.8
Gravity coefficient	g/(m·s^{-2})	9.8
Viscosity of alloy melt	η/(Pa·s)	1.25×10^{-3}
Latent heat	L_m/(kJ·kg^{-1})	396.1

3 Results

3.1 Relevant laws of magnetic fields and magnetic force

Firstly, by using a small TMF generator, we simulated the magnetic fields in the alloy melt during the SS process; meanwhile, we measured and verified the results by a Tesla-meter. The intensity of magnetic fields along longitudinal direction shown in Fig. 2(a) indicates an edge effect [34] appearing in the alloy melt. In other words, the magnetic field intensity is relatively stable in the middle position of magnetic field action space and decreases sharply at both ends. Therefore, during SS process, the mushy zone of alloy melt should be kept in the middle position of magnetic fields generator along the longitudinal direction by the constant downward drag velocity (v_d). In addition, the changes in excitation current parameters, including the intensity and the frequency, will affect the values of induced current

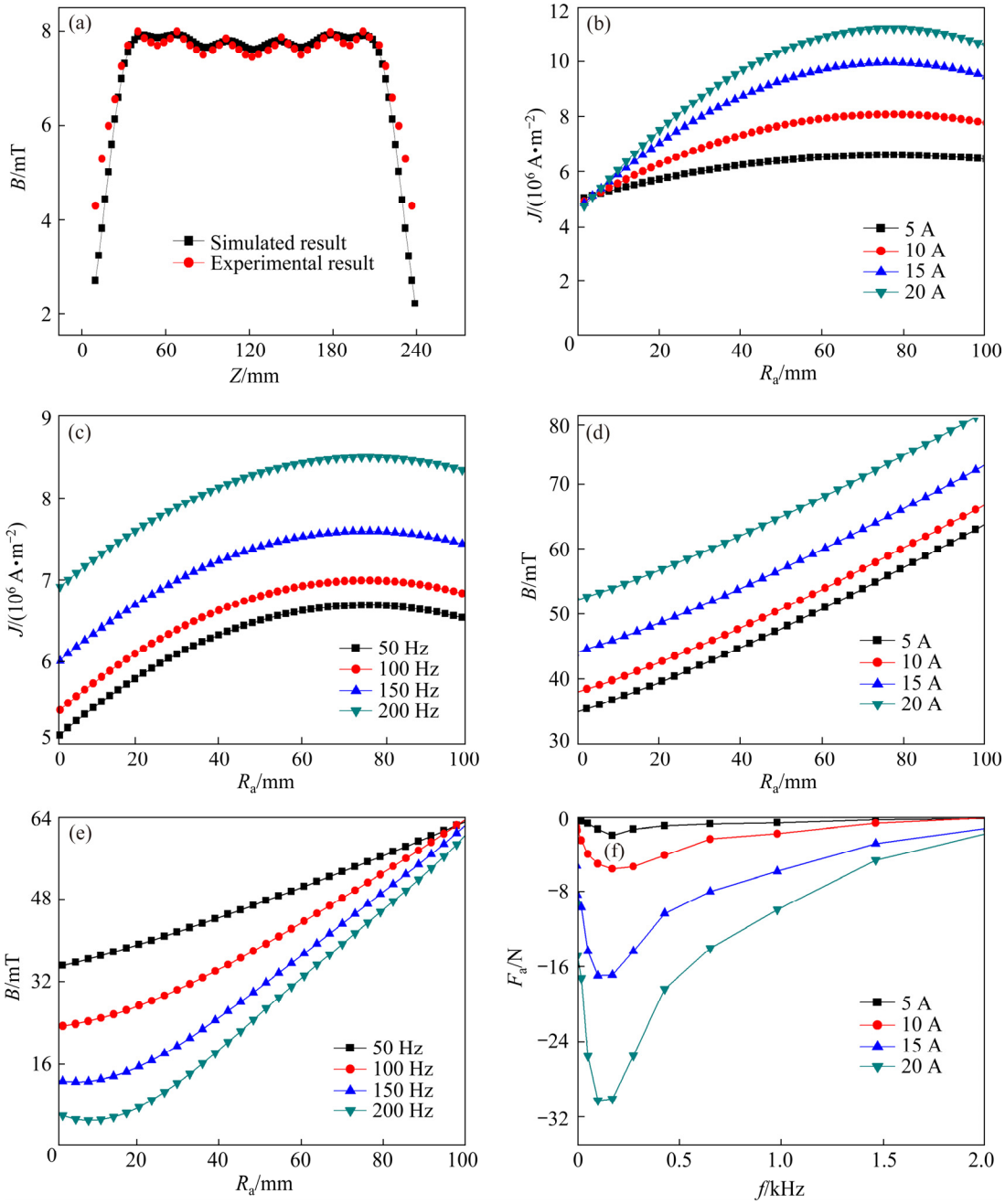

Fig. 2 Correlation law of TMF: Axial distribution of TMF (a), induced current density at different currents (b) and frequencies (c), magnetic field intensity at different currents (d) and frequencies (e), magnetic field force at different currents and frequencies (f) (B denotes magnetic intensity of TMF; J denotes induced current density; R_a denotes radius of alloys; F_a denotes average magnetic force)

density, magnetic intensity and magnetic force in the alloy melt, as well as their distributions in the alloy melt.

From Figs. 2(b) and (d), it can be concluded that magnifying the excitation current can largely improve the intensity of induced current density and magnetic fields in the alloy melt. Additionally, by enhancing the frequency of excitation current, the induced current will be increased largely (Fig. 2(c)). Oppositely, the magnetic intensity will decrease as the frequency of excitation current increases (Fig. 2(e)). Besides, along the radial direction, the intensity of induced current density and magnetic fields are increased as the distance to the side walls decreases, and will maximize at the side walls of TMF generator. Similarly, the magnetic force is

also influenced by the different excitation currents and frequencies. As shown in Fig. 2(f), the maximum of average magnetic force can be greatly improved by about 16 times with the increase of current from 5 to 20 A. Nonetheless, with increasing the frequency from 0 to 2000 Hz, the average magnetic force first increases and then decreases, and turning out to be the maximum at 200 Hz. Accordingly, under our study conditions, we confirmed the excitation current parameters of 20 A and 200 Hz to be the optimal parameters for the generation of TMF with the purpose of providing a more effective magnetic force in the alloy melt. In addition, the optimal area for TMF to process the alloy melt is adjacent to the side walls of the TMF generator; in this regard, the alloy castings with large thin-walled shape can be processed more efficiently by TMF than the castings with other shapes.

3.2 Influence of TMF on elimination of shrinkage defect

The average magnetic force calculated suing the Ansoft-Maxwell was imported into ESI-Procast software for the simulations of SS process, and the results are shown in Fig. 3. Among them, the

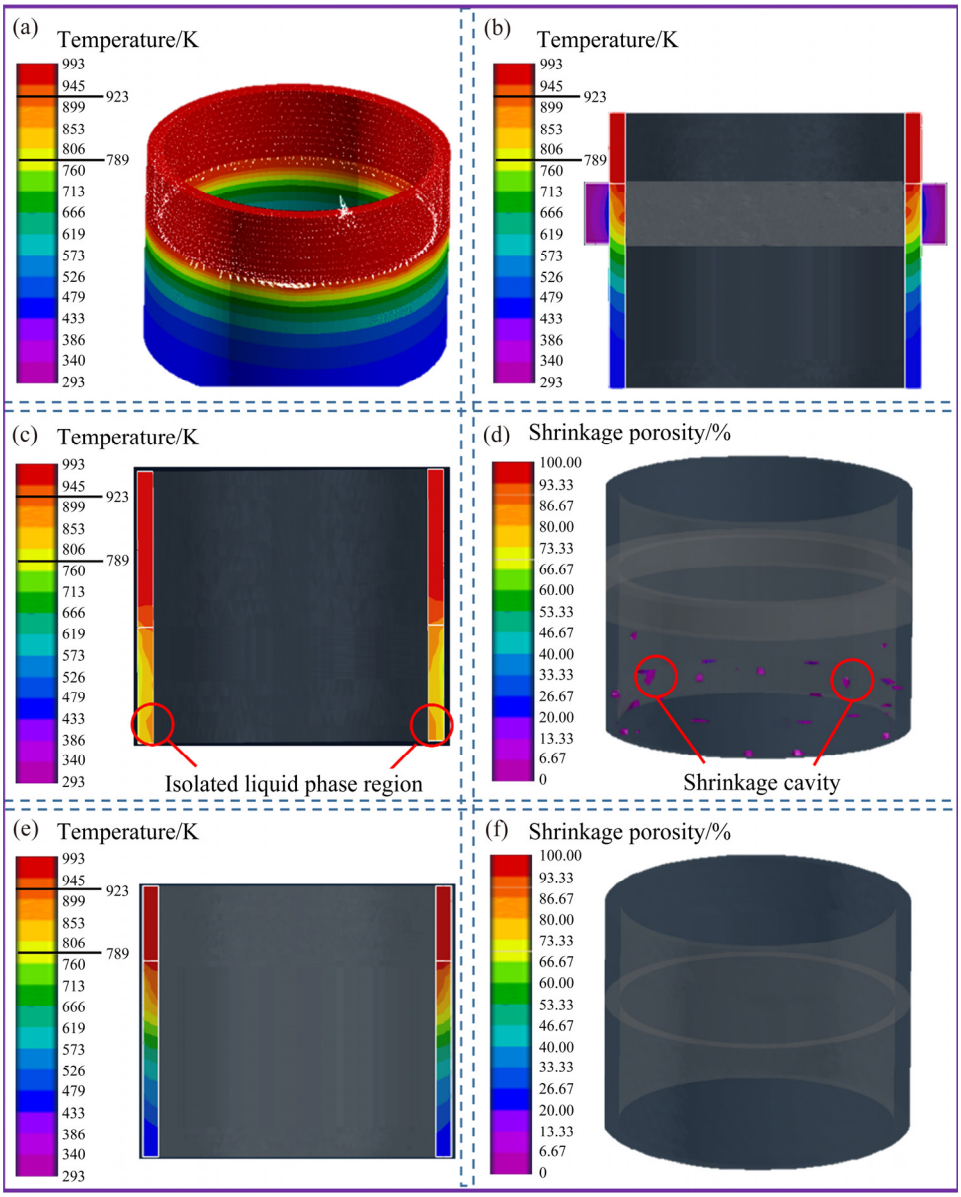

Fig. 3 Simulation model of SS with or without TMF: (a) Distribution of overall temperature in SS casting model; (b) Distribution of side-walls temperature in SS casting model; (c) Solidification behavior during SS; (d) Porosity of SS casting model; (e) Solidification behavior during SS with TMF process; (f) Porosity of SS casting model with TMF process

models in Figs. 3(a) and (b) are the temperature distributions in the whole casting and in the sections of side walls during the SS process, respectively.

It is visible from Fig. 3(c) that the temperature distributions are unidirectional and the values increase from bottom to the top position along the longitudinal direction, which are consistent with the characteristic of sequential solidification process. Besides, in the SS process without TMF, the temperature distributions in the sections of side walls indicate that the isolated liquid phase regions will appear in the alloy castings, which are surrounded by the solid phase regions (Fig. 3(c)). Under the circumstances, the alloy melt cannot flow into the isolated liquid phase regions or feed the regions, so as to form the shrinkage cavity or the porosity at the alloy castings. Therefore, in Fig. 3(d), quantities of shrinkage defects occur at the side walls of the casting, and the porosity reaches about 10%. Here, we used the Niyama criterion [35,36] to represent the quantity of shrinkage defects. It is noteworthy that when TMF is applied into the SS process, the general trend of temperature distributions will not be changed, but the isolated liquid phase region no longer occurs (Fig. 3(e)). This result suggests that the movement and the feeding capacity of the alloy melt in the mushy zones have been significantly increased by TMF process. Additionally, from Fig. 3(f), it can be illustrated that the shrinkage defects in the castings have completely disappeared, which also strongly confirms that TMF process can effectively reduce the shrinkage defects for the large thin-walled castings prepared by ZL205A alloys with large solidification intervals.

In order to further verify the above simulated results, we carried out the related experiments based on the parameters of simulation. Firstly, we selected the same position at the side walls of the castings to observe the macrostructure and microstructure, as exhibited in Fig. 4. Comparing Figs. 4(a) and (b), it is clear that a series of shrinkage defects are formed in the alloy castings by the SS process without TMF. While, when TMF is applied, the shrinkage defects are largely eliminated. Furthermore, from Figs. 4(c) and (d), it can also be demonstrated that in the microstructures, the number of shrinkage defects is decreased greatly by the TMF process. In addition, the microstructure in Fig. 4(d) also presents an obvious sequential growth of dendrites with the TMF process; nevertheless, the growth of dendrites in the process without TMF will form a certain deflection due to natural convection in the alloy melt (Fig. 4(c)). Therefore, the addition of TMF can efficaciously reduce the shrinkage defects in both the macrostructure and microstructure, and promote the sequential growth of dendrites along the direction of temperature gradient.

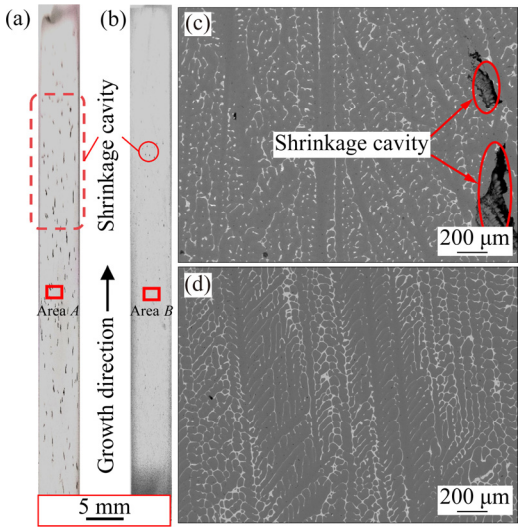

Fig. 4 Shrinkage defects in alloys: (a) Without TMF; (b) TMF process with excitation current of 20 A; (c) Enlarged image of Area *A*; (d) Enlarged image of Area *B*

3.3 Influence of TMF on mechanical performance

We selected the same position of castings to perform the measurements of the tensile, micro-hardness and porosity, and to analyze the fracture morphologies, of which the relevant results are shown in Fig. 5. Wherein, the porosity was calculated by [37]

$$P_p=1-\rho_s/\rho_0 \quad (2)$$

where P_p is the porosity of alloy casting caused by shrinkage defects, ρ_s is the density of the alloy casting measured by the related instrument, and ρ_0 is the theoretical density of alloys. It can be obtained that, the porosity sharply decreases from 1.71% (without TMF) to 0.22% (with TMF and the excitation current of 20 A). Additionally, the ultimate tensile strength and micro-hardness can be significantly improved from 186 MPa and 82.1 kg/mm^2 (without TMF) to 221 MPa and 100.5 kg/mm^2 (with TMF and the excitation current

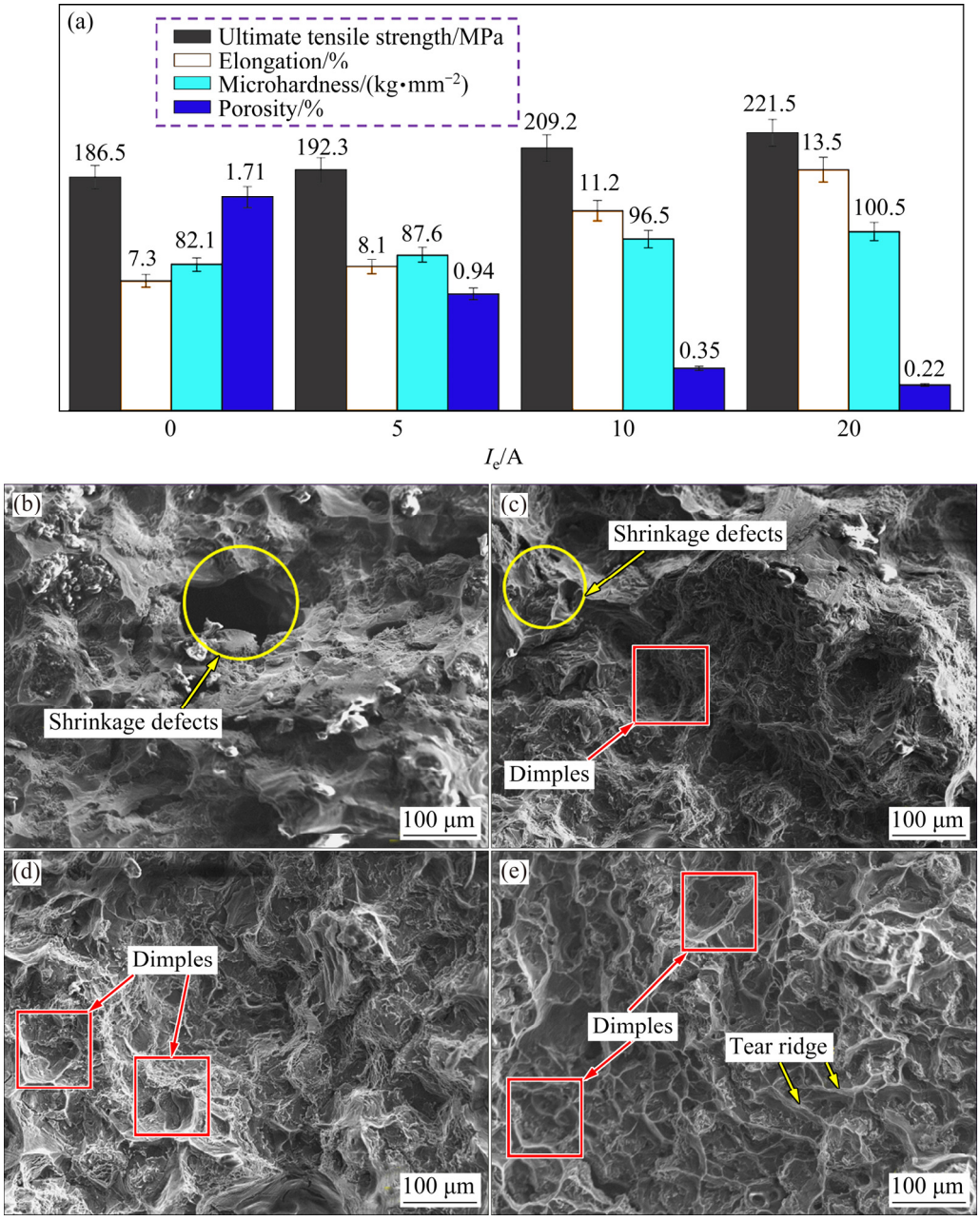

Fig. 5 Performance test (a) and fracture morphologies of alloys with excitation current of 0 A (b), 5 A (c), 10 A (d) and 20 A (e)

of 20 A). Similarly, the elongation increases from 7.3% to 11.7%, which confirms that TMF can promote the ductility of the alloy. Furthermore, these improvements are more significant with the increase of excitation current from 0 to 20 A.

Moreover, the SEM images of fracture morphologies in Fig. 5(b) reveal that there are so many shrinkage cavities and aggregative precipitated phases in the alloys without TMF process; wherein, the dimples are rare and the fracture mode is brittle. With the increase of excitation current, the magnetic field intensity can be increased; subsequently, the porosities are gradually eliminated and the precipitated phases can be uniformly distributed. Contrastively, the dimples are substantially increased and the fracture modes change from brittle mode to ductile mode by the TMF process (Figs. 5(c), (d) and (e)). In summary, TMF can effectively optimize the macrostructure and microstructure, promote the growth of dendrites along the direction of temperature gradient, remove the shrinkage defects, and improve the mechanical properties of the large thin-walled castings prepared by ZL205A alloys with large solidification intervals;

additionally, the improvement effects of TMF will be enlarged with the increase of magnetic fields intensity.

4 Discussion

4.1 Distribution of magnetic force in alloy melt

Many literatures have shown that, the magnetic force is mainly related to the induced current density and magnetic intensity, which will be influenced by the excitation current. The area of TMF can be assumed as a complete alloy casting, so the relationship between the magnetic force and the excitation current can be expressed as [38−41]

$$J_0=I_e/S \tag{3}$$

$$J=J_0\exp(-d/d_s) \tag{4}$$

$$B=\frac{\mu_0 I_e}{2r} \tag{5}$$

$$F=JB \tag{6}$$

where J_0 is the induced current density on the alloy casting surface, J is the induced current density inside the alloy casting, S is the cross-sectional area of the electromagnetic coil, d is the distance to the coil, d_s is the depth of skin effect dependent on the alloy casting, B is the magnetic intensity, μ_0 is the permeability of vacuum, r is the radius of coil and equal to d here, and F is the magnetic force. From Eqs. (3) and (4), we can obtain that the induced current density inside the alloy casting will be enlarged with the increase of excitation current intensity, but will be decreased with the increase of the distance to the coil. Similarly, Eq. (5) also indicates that the magnetic intensity is positively correlated with the excitation current, but is negatively correlated with the radius of coil, i.e., equal to d. Consequently, both the induced current density and magnetic intensity will increase as the distance to the magnetic fields generator decreases, and reach the maximum at the side wall of magnetic fields generator. In addition, we can conclude from Eq. (6) that the magnetic force can increase dramatically as the excitation current increases, likewise, it will increase with the decrease of distance to the magnetic fields generator, finally reach the maximum at the side walls of TMF generator. Therefore, the results shown in Fig. 2 are verified. Furthermore, it can be demonstrated that the alloy castings with large thin-walled shape can be processed more efficiently by TMF than the castings with other shapes. Besides, when the alloy casting has a large thin-walled shape, the value of J is the same as J_0, so that Eq. (6) can be converted to

$$F=(I_e/S)\times\frac{\mu_0 I_e}{2r} \tag{7}$$

Therefore, it can be easily obtained that the magnetic force is positively correlated with the square of current, as demonstrated in Fig. 2. In addition, the excitation current has a close association with frequency (f), as

$$I_e=I_0\sin\left(2\pi ft+\varphi\right) \tag{8}$$

where I_0 is the maximum current, f is the current frequency, φ is the phase angle and t is the time. It can be calculated that the current and frequency have a sinusoidal relationship, so that there can be a specific frequency value that maximizes the current, in turn to maximize the magnetic field strength and magnetic force, as shown in Fig. 2.

4.2 Effect of TMF on elimination of shrinkage defect

To analyze the shrinkage behavior in the solidification process, we established the sequential solidification models, as shown in Fig. 6. In this case, the transverse sections of the feeding channels are considered to be circular sections, of which the radius will decrease with the increase of solid phase fraction. The alloy melt in the feeding channels can form the continuous laminar flows, and the feeding capacity can be affected by the solidified rate and dynamic conditions. When the feeding channels are small and the feeding rate is less than the solidified rate, the feeding behavior will be difficult to continue, resulting in isolated liquid phase regions surrounded by the solid phase regions. As a result, the isolated liquid phase regions cannot be fed during the solidification, and the shrinkage defects are formed. On the other hand, with respect to the dynamic conditions, the change of pressure in the alloy melt will also influence the feeding behavior during the SS process, as follows [42−44]:

$$\Delta P_s=\sigma R^{-1} \tag{9}$$

where ΔP_s is the increased pressure generated by the surface tension, σ is the surface tension of alloy melt in the feeding channels, and R is the radius of cross section of the feeding channels. Additionally, the increased pressure induced by the volume force (ΔP_v) can be expressed as [42−44]

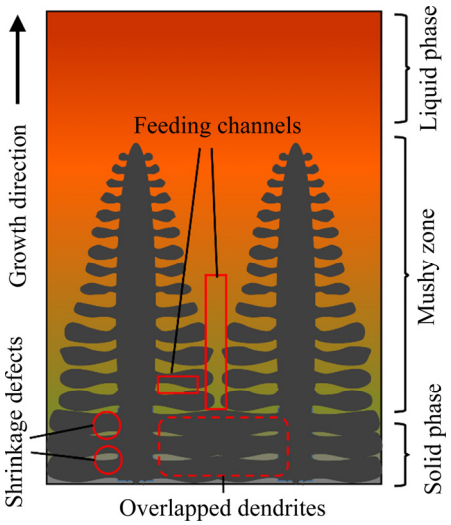

Fig. 6 Solidification behavior of alloy melt in SS process [42]

$$\Delta P_v=(\rho g+F_m)L \tag{10}$$

where ρ is the density of alloy melt, g is the gravity coefficient, F_m is the magnetic force, and L is the length that can be reached by the feeding capacity in the feeding channels. However, in the solidification process, the growth of dendrites will produce a reduction in feeding pressure (ΔP_f), as follows [42−44]:

$$\Delta P_f=\int_0^L 8u\eta R^{-2}\mathrm{d}L \tag{11}$$

where u is the feeding rate of alloy melt, and η is the viscosity of alloy melt. Since the melt flows formed in the feeding channels are continuous, Eq. (11) can be evolved as

$$\Delta P_f=8u\eta R^{-2}L \tag{12}$$

Therefore, according to the law of conservation of energy, following formulas can be obtained [42]:

$$P_l-P_0+\Delta P_s+\Delta P_v-\Delta P_f=0 \tag{13}$$

$$L=(P_l-P_0)/(8u\eta R^{-2}-\rho g-F_m) \tag{14}$$

where P_0 is the static pressure at the beginning of the feeding channels, and P_l is the pressure at a position of L in the feeding channels. Moreover, the values of the constant parameters including ρ, g and η are listed in Table 1. By combining Eqs. (10)−(14), it can be confirmed that with the increase of F_m, the length L representing the feeding capacity will be increased accordingly. That is, TMF during the SS process is very effective to increase the feeding pressure in the feeding channels, further to improve the feeding capacity of alloy melt in the mushy zone, so as to reduce the shrinkage defects for alloys with large solidification intervals.

Additionally, ZL205A alloys as the Al−Cu based alloys with large solidification intervals, will have a low critical velocity for the steady growth of a flat solid−liquid interface during solidification, which can easily produce the instability of interface to form cellular and dendritic crystals [6−8]. In this case, the distribution of temperature and solute will be serious chaotic, and the growth of dendrites will be deflected and disordered. Meanwhile, secondary dendrites will be relatively developed [45]. As a result, the feeding channels between the dendrites in the mushy zones become easily blocked and the feeding capacity is decreased, so as to badly form the isolated liquid phase regions (Fig. 3(c)) and the shrinkage defects (Fig. 3(d) and Figs. 4(a, b)) during the sequential solidification process. Comparatively, according to the previous work, it can be indicated that the TMF can generate the strong long-range sequential melt flows by the combination of gravity, buoyancy, Marangoni forces and the Lorentz forces [27]. Moreover, these melt flows can effectively regulate the heat and mass transfer, in turn to distribute the temperature and solute in the alloy melt more uniform and stable. In this case, the isolate liquid phase can be removed (Fig. 3(e)), and the feeding capacity can be enhanced, so that the shrinkage defects can be eliminated availably (Fig. 3(f) and Figs. 4(c, d)). Besides, the strong melt flows induced by TMF can crush and break up the secondary dendrite arms [46,47], so as to reduce the formation of secondary dendrites and overlaps, further to largely widen the feeding channels. Hence, the solidification rate is decreased, and the feeding time is delayed. Consequently, TMF can widen the feeding channels and prolong the feeding time, leading to an increase of feeding capacity of alloy melt in the mushy zone during the SS process.

4.3 Effect of TMF on mechanical performance

The effect of TMF on optimization of shrinkage defects and microstructure is mainly

determined by the value of magnetic force, in other words, the intensity of excitation current (as discussed in Eq. (7)). When the intensity of excitation current increases, the intensity of TMF and the magnetic force can be enhanced accordingly, so that the efficiency of the sequential transfer of mass and heat will be improved, as well as the feeding capacity. Meanwhile, the growth of matrix phase α(Al) along the direction of temperature gradient can be promoted effectively, and the crushing capacity to the secondary dendrites and overlaps will be increased accordingly, as the intensity of excitation current increases (Fig. 4). Consequently, the elimination of shrinkage defects and the optimization of microstructure can be more efficient when the intensity of excitation current is large (Fig. 5). Therefore, with the increase of the intensity of excitation current, the formation of shrinkage defects can be correspondingly reduced, and the grain size will be refined effectively, further to greatly increase the tensile strength and the micro-hardness. Additionally, the growth of matrix phase α(Al) along the direction of temperature gradient can be improved and uniformed, so as to increase the elongation of alloy castings. In summary, TMF can increase the feeding capacity of alloy melt in the mushy zone during the SS process, promote and uniform the growth of of matrix phase α(Al) along the direction of temperature gradient and reduce the secondary dendrites and overlaps. Ultimately, the TMF process can eliminate the shrinkage defects and optimize the microstructure, in turn to effectively improve the mechanical performance.

5 Conclusions

(1) Magnetic force can be increased with the increase of the exciting current, while as the exciting current frequency increases, it will first increase and then decrease, and reach the maximum value at 200 Hz. Additionally, the magnetic force increases as the distance to the side walls of TMF generator decreases, so as to more easily regulate the alloy castings with large thin-walled shape.

(2) TMF can significantly improve the feeding capacity of alloy melt by breaking the secondary dendrites and overlaps between dendrites, prolonging the feeding time, optimizing the feeding channels and promoting the growth of dendrites along the direction of temperature gradient.

(3) TMF coupling with SS process can effectively eliminate the shrinkage defects and improve the mechanical performance of alloys. Specifically, this process can increase the ultimate tensile strength, elongation and microhardness of alloys from 186 MPa, 7.3% and 82.1 kg/mm^2 without TMF to 221 MPa, 11.7% and 100.5 kg/mm^2 under TMF process with an excitation current of 20 A, while decrease the porosity from 1.71% to 0.22%; meanwhile, it can alter the brittle fracture mode to ductile fracture mode.

Acknowledgments

The authors are grateful for the financial supports from the National Key Research and Development Program of China (2017YFA0403804) and the National Natural Science Foundation of China (51425402, 51671073).

References

[1] PATEL M, QIU Dong, WANG Gui, GIBSON M, PRASAD A, STJOHN D H, EASTON M A. Understanding the refinement of grains in laser surface remelted Al−Cu alloys [J]. Scripta Materialia, 2020, 178: 447−451.

[2] SHAGA A, SHEN Ping, XIAO Li-guang, GUO Rui-fen, LIU Ya-bing, JIANG Qi-chuan. High damage-tolerance bio-inspired ZL205A/SiC composites with a lamellar-interpenetrated structure [J]. Materials Science and Engineering A, 2017, 708(21): 199−207.

[3] LI Bo, SHEN Yi-fu, HU Wei-yue. Casting defects induced fatigue damage in aircraft frames of ZL205A aluminum alloy—A failure analysis [J]. Materials and Design, 2011, 32(5): 2570−2582.

[4] WANG Ru-jia, WU Shi-ping, CHEN Wei. Mechanism of burst feeding in ZL205A casting under mechanical vibration and low pressure [J]. Transactions of Nonferrous Metals Society of China, 2018, 28(8): 1514−1520.

[5] HAN S, CHO H, JIN S Y, SEDEN M, LEE I, SOHN I. Effects of simultaneous static and traveling magnetic fields on the molten steel flow in a continuous casting mold [J]. Metallurgical and Materials Transactions B, 2018, 49(5): 2757−2769.

[6] DU Da-fan, HOU Long, GAGNOUD A, REN Zhong-ming, FAUTRELLE Y, CAO Guang-hui, LI Xi. Effect of an axial high magnetic field on Sn dendrite morphology of Pb−Sn alloys during directional solidification [J]. Journal of Alloys and Compounds, 2014, 588: 190−198.

[7] ROSALIE J, BOURGEOIS L. Silver segregation to θ'(Al_2Cu)−Al interfaces in Al−Cu−Ag alloys [J]. Acta Materialia, 2012, 60: 6033−6041.

[8] GAO Lin, OU Xiao-qin, NI Song, LI Kai, DU Yong, SONG Min. Effects of θ' precipitates on the mechanical performance and fracture behavior of an Al−Cu alloy

subjected to overaged condition [J]. Materials Science and Engineering A, 2019, 762: 138091.

[9] LIU Gang, SUN Jun, NAN Ce-wen, CHEN Kang-hua. Experiment and multiscale modeling of the coupled influence of constituents and precipitates on the ductile fracture of heat-treatable aluminum alloys [J]. Acta Materialia, 2005, 53(12): 3459−3468.

[10] QU Min, LIU Lin, CUI Yan, LIU Feng-bin. Interfacial morphology evolution in directionally solidified Al−1.5%Cu alloy [J]. Transactions of Nonferrous Metals Society of China, 2015, 25(2): 405−411.

[11] THIEME N, KEIL M, MEIER D, BÖNISCH P, DADZIS K, PÄTZOLD O, STELTER M, BÜTTNER L, CZARSKE J. Directional solidification of gallium under time-dependent magnetic fields with in situ measurements of the melt flow and the solid−liquid interface [J]. Journal of Crystal Growth, 2019, 522: 221−229.

[12] LEE P, HUNT J. Hydrogen porosity in directionally solidified aluminium−copper alloys: A mathematical model [J]. Acta Materialia, 2001, 49(8): 1383−1398.

[13] FERREIRA I, SIQUEIRA C, SANTOS C, GARCIA A. Theoretical and experimental analysis of inverse segregation during unidirectional solidification of an Al−6.2wt.%Cu alloy [J]. Scripta Materialia, 2003, 49(4): 339−344.

[14] XU Bin, RUI Zhi-yuan. Moldflow-based optimization design of gating system in injection mold for automobile bumper [J]. Advanced Materials Research, 2014, 1061−1062: 465−470.

[15] ZHANG Jia-ying, ZUO Li-jie, FENG Jian, YE Bing, KONG Xiang-yang, JIANG Hai-yan, DING Wen-jiang. Effect of thermal exposure on microstructure and mechanical properties of Al−Si−Cu−Ni−Mg alloy produced by different casting technologies [J]. Transactions of Nonferrous Metals Society of China, 2020, 30(7): 1717−1730.

[16] REYNA J, GARCIA M, CRUZ V, CURIEL F, DZIB L, FALCON L. Effect of electromagnetic interaction on microstructure and corrosion resistance of 7075 aluminium alloy during modified indirect electric arc welding process [J]. Transactions of Nonferrous Metals Society of China, 2019, 29(3): 473−484.

[17] WANG Pei, ECKERT J, PRASHANTH K, WU Ming-wei, KABAN I, XI Li-xia, SCUDINO S. A review of particulate-reinforced aluminum matrix composites fabricated by selective laser melting [J]. Transactions of Nonferrous Metals Society of China, 2020, 30(8): 2001−2034.

[18] ALEXANDROV D, GALENKO P. Dendrite growth under forced convection: Analysis methods and experimental tests [J]. Physics Uspekhi, 2014, 57(8): 771−786.

[19] GAO Jian-rong, HAN Meng-kun, KAO A, PERICLEOUS K, ALEXANDROV D, GALENKO P. Dendritic growth velocities in an undercooled melt of pure nickel under static magnetic fields: A test of theory with convection [J]. Acta Materialia, 2016, 103(15): 184−191.

[20] WEI Hai-gen, XIA Fu-zhong, QIAN Shen, WANG Ming-pu. Effect of permanent magnetic stirring on the solidification microstructure and ingot quality of Al−Cu alloys [J]. Journal of Materials Processing Technology, 2017, 240: 344−353.

[21] WANG Feng, ESKIN D, MI Jia-wei, WANG Chuang-nan, KOE B, KING A, REINHARD C, CONNOLLEY T. A synchrotron X-radiography study of the fragmentation and refinement of primary intermetallic particles in an Al−35Cu alloy induced by ultrasonic melt processing [J]. Acta Materialia, 2017, 141: 142−153.

[22] BADIZI R, PARIZAD A, ASKARI M, SHAHVERDI R. Optimization of mechanical properties using D-optimal factorial design of experiment: Electromagnetic stir casting process of A357−SiC nanocomposite [J]. Transactions of Nonferrous Metals Society of China, 2020, 30(5): 1183−1194.

[23] AVNAIM M, MIKHAILOVICH B, AZULAY A, LEVY A. Numerical and experimental study of the traveling magnetic field effect on the horizontal solidification in a rectangular cavity, part 2: Acting forces ratio and solidification parameters [J]. International Journal of Heat and Fluid Flow, 2018, 69: 23−32.

[24] KESAVAN V, SRINIVASAN M, RAMASAMY P. Numerical investigation of directional solidification process for improving multi-crystalline silicon ingot quality for photovoltaic applications [J]. Materials Letters, 2019, 241: 180−183.

[25] LIOTTI E, LUI A, KUMAR S, GUO Z, BI C, CONNOLLEY T, GRANT P. The spatial and temporal distribution of dendrite fragmentation in solidifying Al−Cu alloys under different conditions [J]. Acta Materialia, 2016, 121: 384−395.

[26] MATHIESEN R, ARNBERG L, BLEUET P, SOMOGYI A. Crystal fragmentation and columnar-to-equiaxed transitions in Al−Cu studied by synchrotron X-ray video microscopy [J]. Metallurgical and Materials Transactions A, 2006, 37(8): 2515−2524.

[27] LUO Lei, LUO Liang-shun, RITCHIE R, SU Yan-qing, WANG Bin-bin, WANG Liang, CHEN Rui-run, GUO Jing-jie, FU Heng-zhi. Optimizing the microstructures and mechanical properties of Al−Cu-based alloys with large solidification intervals by coupling travelling magnetic fields with sequential solidification [J]. Journal of Materials Science & Technology, 2021, 61: 100−113.

[28] PENG Lan, GONG Huan. Effects of static magnetic fields on melt flow in detached solidification [J]. Transactions of Nonferrous Metals Society of China, 2015, 25(3): 936−943.

[29] AVNAIM M, MIKHAILOVICH B, AZULAY A, LEVY A. Numerical and experimental study of the traveling magnetic field effect on the horizontal solidification in a rectangular cavity, part 1: Liquid metal flow under the TMF impact [J]. International Journal of Heat and Fluid Flow, 2018, 69: 23−32.

[30] WANG Jiang, YUE Sheng, FAUTRELLE Y, LEE P, LI Xi, ZHONG Yun-bo, REN Zhong-ming. Refinement and growth enhancement of Al_2Cu phase during magnetic field assisting directional solidification of hypereutectic Al−Cu alloy [J]. Scientific Reports, 2016, 6: 24585.

[31] XU Yan-jin, WEI Li-jun, HAN Bao-shuai, GUO En-yu, WANG Ming-yue, SU yan-qing. Effect of a traveling magnetic field on micropore formation in Al−Cu alloys [J]. Metals, 2018, 8(6): 448.

[32] OU Yuan, SHUAI San-san, DONG Yua-hao, XUAN Wei-dong, WANG Jiang, ZHANG Zhen-qiang, REN Xin-gfu, REN Zhong-ming. Effect of thermoelectric magnetic

convection on shrinkage porosity at the final stage of solidification of GCr18Mo steel under axial static magnetic field [J]. Metallurgical and Materials Transactions B, 2019, 59(2): 881−889.

[33] ZIMMERMAN G, PICKMANN C, HAMACHER M, ZIMMERMANN E, HEYME H, ECKERT K, ECKERT S. Fragmentation-driven grain refinement in directional solidification of AlCu10wt% alloy at low pulling speeds [J]. Acta Materialia, 2017, 126: 236−250.

[34] DADZIS K, LUKIN G, MEIER D, BÖNISCH P, SYLLA L, PÄTZOLD O. Directional melting and solidification of gallium in a traveling magnetic field as a model experiment for silicon processes [J]. Journal of Crystal Growth, 2016, 445: 90−100.

[35] NIYAMA E, UCHIDA T, MORIKAWA M, SAITO S. Predicting shrinkage in large steel castings from temperature gradient calculations [J]. International Journal of Cast Metals Research, 1981, 6(2): 16−22.

[36] NIYAMA E, UCHIDA T, MORIKAWA M. A method of shrinkage prediction and its application to steel casting practice [J]. International Journal of Cast Metals Research, 1982, 7: 52−63.

[37] BOEIRA A, FERREIRA I, GARCIA A. Alloy composition and metal/mold heat transfer efficiency affecting inverse segregation and porosity of as-cast Al−Cu alloys [J]. Materials and Design, 2009, 30(6): 2090−2098.

[38] DADZIS K, VIZMAN D, FRIEDRICH J. Unsteady coupled 3D calculations of melt flow, interface shape, and species transport for directional solidification of silicon in a traveling magnetic field [J]. Journal of Crystal Growth, 2013, 367(15): 77−87.

[39] DADZIS K, EHRIG J, NIEMIETZ K, PÄTZOLD O, WUNDERWALD U, FRIEDRICH J. Model experiments and numerical simulations for directional solidification of multicrystalline silicon in a traveling magnetic field [J]. Journal of Crystal Growth, 2011, 333: 7−15.

[40] YU Qing-hua, LIU Li-jun, LI Zao-yang, SHAO Yue. Parameter study of traveling magnetic field for control of melt convection in directional solidification of crystalline silicon ingots [J]. International Journal of Heat and Fluid Flow, 2018, 71: 55−67.

[41] XU Yan-jin, SU Yan-qing, LUO Liang-shun, LI Xin-zhong, LIU Jiang-ping, GUO Jing-jie, CHEN Rui-run, FU Heng-zhi. Effect of traveling magnetic field on gas porosity during solidification [J]. Transactions of Nonferrous Metals Society of China, 2011, 21(9): 1981−1985.

[42] LUO Lei, LUO Liang-shun, SU Yan-qing, SU Lin, WANG Liang, GUO Jing-jie, FU Heng-zhi. Optimizing the microstructure, shrinkage defects and mechanical performance of ZL205A alloys via coupling travelling magnetic fields with unidirectional solidification [J]. Journal of Materials Science & Technology, 2021, 74: 246−258.

[43] WANG Ye, WU Shi-ping, XUE-Xiang, CHEN Rui-run, ZHANG Jian-bin, XIAO Wen-feng. Formation mechanism and criterion of linear segregation in ZL205A alloy [J]. Transactions of Nonferrous Metals Society of China, 2014, 24(11): 3632−3638.

[44] GAO Zhi-ming, JIE Wang-qi, LIU Yong-qin, LUO hai-jun. Solidification modelling for coupling prediction of porosity and segregation [J]. Acta Materialia, 2017, 127(1): 277−286.

[45] LIU Zheng, ZHANG Si-bo, MAO Ping-li, WANG Feng. Effects of Y on hot tearing susceptibility of Mg−Zn−Y−Zr alloys [J]. Transactions of Nonferrous Metals Society of China, 2014, 24(4): 907−914.

[46] WANG Lei, SHEN Jun, WANG Ling-shui, FENG Zhou-rong, FU Heng-zhi. Effect of travelling magnetic field on interface morphology in directionally solidified Sn−Cd alloy [J]. Transactions of Nonferrous Metals Society of China, 2013, 23(8): 2454−2459.

[47] MIN Zhi-xian, SHEN Jun, WANG Ling-shui, LIU Lin. Effect of traveling magnetic field on dendrite growth of Pb−Sn alloy during directional solidification [J]. Transactions of Nonferrous Metals Society of China, 2011, 21(9): 1976−1980.

行波磁场耦合顺序凝固改善 ZL205A 大型薄壁件缺陷及性能

罗 磊，夏宏营，骆良顺，苏彦庆，蔡超军，王 亮，郭景杰，傅恒志

哈尔滨工业大学 材料科学与工程学院 金属精密热加工国家重点实验室，哈尔滨 150001

摘 要：利用行波磁场耦合顺序凝固连续地处理大型薄壁 ZL205A 合金铸件，消除收缩缺陷，提高力学性能。实验结合模拟，针对行波磁场参数优化对补缩行为、显微组织和性能的影响进行系统的研究。结果表明，本研究条件下，当励磁电流为 20 A、频率为 200 Hz 时，磁场力达到最大值；磁场力随着到磁场发生器距离越近而越大，更有利于对薄壁铸件进行处理。行波磁场可以有效破碎二次枝晶臂和枝晶间的搭接，拓宽补缩通道，延长补缩时间，优化补缩路径，最终消除收缩缺陷并提高力学性能。当励磁电流为 20 A 时，铸态合金极限抗拉强度、伸长率和显微硬度分别由 186 MPa、7.3%和 82.1 kg/mm^2 提高至 221 MPa、11.7%和 100.5 kg/mm^2，孔隙率由 1.71%降至 0.22%，断裂模式由脆性转变为韧性断裂。

关键词：ZL205A 合金；大型薄壁合金铸件；行波磁场；顺序凝固；收缩缺陷；力学性能

(Edited by Xiang-qun LI)